Ignition of dimethyl ether/air mixtures by hot particles: Impact of low temperature chemical reactions

Yiqing Wang [a], Huangwei Zhang [b], Thorsten Zirwes [c,d], Feichi Zhang [d], Henning Bockhorn [d], Zheng Chen [a,*]

[a] *SKLTCS, CAPT, BIC-ESAT, College of Engineering, Peking University, Beijing 100871, China*
[b] *Department of Mechanical Engineering, Faculty of Engineering, National University of Singapore, 117575, Singapore*
[c] *Steinbuch Centre for Computing, Karlsruhe Institute of Technology, 76344 Eggenstein-Leopoldshafen, Germany*
[d] *Engler-Bunte Institute/Division of Combustion Technology, Karlsruhe Institute of Technology, 76131 Karlsruhe, Germany*

Abstract

Understanding and characterizing ignition of flammable mixtures by hot particles is important for assessing and reducing the risk of accidental ignition and explosion in industry and aviation. Recently, many studies have been conducted for ignition of gaseous mixtures by hot particles. However, the effects of low-temperature chemistry (LTC) on ignition by hot particles received little attention. LTC plays an important role in the ignition of most hydrocarbon fuels and may induce cool flames. The present study aims to numerically assess the effects of LTC on ignition by the hot particles. We consider the transient ignition processes induced by a hot spherical particle in quiescent and flowing stoichiometric dimethyl ether/air mixtures. 1D and 2D simulations, respectively, are conducted for the ignition process by hot-particles in quiescent and flowing mixtures. A detailed kinetic model including both LTC and high-temperature chemistry (HTC) is used in simulations. The results exhibit a premixed cool flame to be first initiated by the hot particle. Then a double-flame structure with both premixed cool and hot flames is observed at certain conditions. At zero or low inlet flow velocities, the hot flame catches up and merges with the leading cool flame. At high inlet flow velocities, the hot flame cannot be initiated due to the short residence time and large convective loss of heat and radicals. Comparing the results with and without considering LTC confirms that LTC accelerates substantially ignition via HTC in a certain range of hot particle temperatures. The mechanism of ignition promotion by LTC is interpreted by analyzing the radical pool produced by the LTC and HTC surrounding the hot particle. Moreover, the influence of inlet flow velocity on ignition by hot particles is assessed. Non-monotonic change of ignition delay time with flow velocity is observed and discussed.
© 2020 The Combustion Institute. Published by Elsevier Inc. All rights reserved.

Keywords: Hot particle ignition; Low-temperature chemistry; Cool flame; Ignition time

---

* Corresponding author.
  E-mail address: cz@pku.edu.cn (Z. Chen).

1. Introduction

Hot particles, such as mechanical sparks in manufacturing and mining operations, are a typical thermal ignition source [1]. Understanding and characterizing ignition by hot particles is helpful for assessing and reducing the risk of accidental ignition of flammable mixtures in industry and aviation [2,3]. Experiments on this topic go back to the 1930s when Silver [4] measured the minimum ignition temperature for spherical hot particles injected into a combustible mixture. Thereafter, numerous experiments were conducted studying the influence of material and size of particles, particle velocities, mixture composition, and ambient pressure and temperature on the critical ignition conditions [5–12]. In addition, one-dimensional (1D) numerical simulations have been performed and accurately predicted the ignition temperature for stationary particles [10,13]. Recently, due to the development of experimental techniques and computing power, more attention has been paid to the kinetics and dynamics of ignition by hot particles. Coronel et al. [3,14,15] developed an experimental technique to accurately characterize the ignition process induced by a hot particle falling into a flammable mixture. They used shearing interferometry to visualize the ignition kernel formation and subsequent flame propagation. Melguizo-Gavilanes et al. [16] conducted 2D numerical simulations for this configuration and found that boundary layer development and flow separation play important roles in the ignition process. Zirwes et al. [17] performed 2D and 3D numerical simulations to study the ignition by hot particles with a broad range of relative velocities between the hot particle and the surrounding mixture. They found that the flow velocity determines the position where the ignition kernel is first formed.

It is well known that chemical reactions occurring at low temperature (Low-Temperature Chemistry, LTC) plays an important role in ignition of most fuels. The LTC may induce a cool flame at certain conditions (see [18] and references therein). For example, the cool flames were observed in droplet combustion and in counterflow system with O_3 addition [19–21]. However, the effects of LTC on hot particle ignition have received little attention in previous studies. In numerical simulations of n-hexane/air ignited by a hot surface, Menon et al. [22] found a two-stage ignition process which is different from that in a homogenous reactor. However, ignition and development of LTC-induced cool flames were not reported in [22]. Coronel et al. [15] conducted 2D numerical simulations of ignition in n-hexane/air mixtures by hot particles. Employing the reaction mechanism of Mével et al. [23], they found that the LTC increases the ignition delay time and ignition temperature. However, these results are counterintuitive since the LTC is expected to promote ignition and reduce the global ignition delay time, at least in a homogeneous ignition system. Currently, the effects of LTC on ignition by hot particles are still not well understood. Particularly, the following questions should be addressed:

(1) Are cool flames initiated during ignition by hot particles?
(2) How does LTC affect the ignition time by hot-particle ignition?
(3) How does LTC couple with relative flow velocity between the hot particle and flammable mixture?

The present study aims to answer these three questions by numerically simulating ignition in dimethyl ether (DME)/air mixtures by hot particles. Specifically, cool flame initiation induced by a hot particle will be addressed and the effects of LTC on hot flame ignition will be assessed. Moreover, the influence of inlet flow velocity and the interaction with LTC during ignition by hot particles will be investigated. Dimethyl ether is considered here since it is an alternative fuel producible from biomass gasification and it has typical two-stage ignition behavior described by relatively well-developed and compact kinetic mechanism.

2. Numerical model and methods

We consider the transient ignition and flame propagation induced by a hot spherical particle in a stoichiometric gaseous DME/air mixture at $P = 1$ atm and $T_u = 480$ K. The hot particle is fixed in space with a constant surface temperature, T_P, to be specified. Its radius is fixed to be $R = 1$ mm since the typical size of mechanical sparks is from a few hundred microns to about 2 mm [24]. We consider both quiescent and flowing DME/air mixtures, so that the interaction between flow velocity and LTC during ignition by hot particles can be studied. Buoyancy is not considered here implying spherical symmetry for the quiescent mixtures and application of 1D numerical simulations. For the ignition by hot spherical particles in a flowing mixture, the problem is axisymmetric and is studied by 2D simulations. The DME chemistry in [25] is used and it includes both LTC and High-Temperature Chemistry (HTC).

The in-house code A-SURF [26] is used to simulate the 1D ignition process. In A-SURF, the finite volume method is used to solve the conservation equations in spherical coordinates. The details on governing equations and numerical methods for A-SURF are presented in [26–28]. The computation domain is $1 \leq r \leq 500$ mm. At the particle surface of $r = R = 1$ mm, an isothermal boundary condition with fixed particle temperature, T_P, as well as zero flow speed and mass diffusion speed, is used. At the outer boundary at
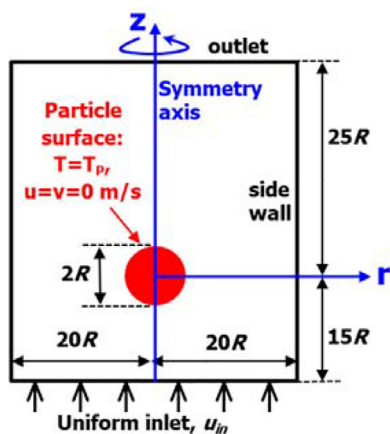
Fig. 1. Schematic of the 2D simulation setup. The particle radius is $R = 1$ mm.

Fig. 2. Contour of total heat release rate in r-t space for (a) $T_P = 1200$ K with LTC, and (b) $T_P = 1425$ K without LTC.

$r = 500$ mm, adiabatic and non-reflective boundary conditions are enforced. Adaptive mesh refinement is used. The finest cell size is $16\,\mu$m and grid convergence is ensured. Section S1 of the Supplementary Document and [37] demonstrates that the hot-particle induced ignition process can be accurately simulated by A-SURF.

For ignition by hot particles in flowing DME/air mixtures, OpenFOAM [29,30] is used for 2D simulations in cylindrical coordinates assuming axial symmetry. The conservation equations in [17] are solved using the finite volume method. The reaction rates, molecular diffusive properties and thermophysical properties are calculated by Cantera [31]. Detailed descriptions of the governing equations, transport model and numerical methods are given in [17]. The configuration presented in Fig. 1 is virtually the same as that considered in [13,17]. In the rectangular computational domain, the hot particle is a sphere fixed at $r = z = 0$. The boundaries are depicted in Fig. 1. At the inlet, the stoichiometric DME/air mixture enters the domain at a prescribed uniform inlet velocity, u_{in}, and the direction along the symmetry axis (i.e., the z axis). At the outlet, zero gradient boundary conditions are applied for all variables except that the wave transmissive boundary condition [32] is used for pressure. Adiabatic wall boundary condition is applied for the side wall. Due to symmetry, only half of the domain in Fig. 1 is considered in the simulations. About 60,000 cells are used and the finest cell near the particle surface has a length of $15.7\,\mu$m. The reaction zone is covered by more than 15 grid points and the grid convergence is ensured. According to [17], flow separation and asymmetric formation of unsteady vortices may appear at large inlet velocities, which requires 3D simulations. Therefore, here the inlet velocity is constrained in the range of $0 \leq u_{in} \leq 1$ m/s so that axis-symmetry is maintained.
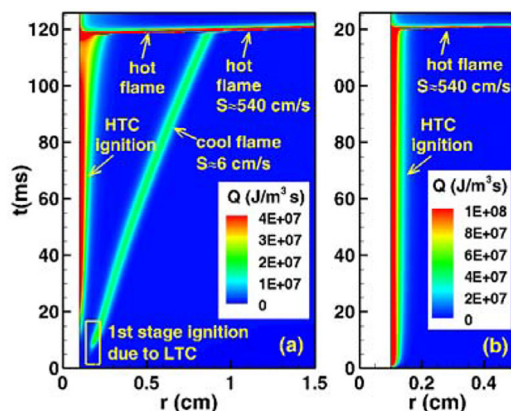
As shown in Section S2 of the Supplementary Document, at zero inlet velocity the results from 2D simulations using OpenFOAM agree very well with those from 1D simulations using A-SURF. This demonstrates the consistency between 1D and 2D simulations. For 1D simulations, A-SURF is used due to its adaptive mesh refinement technique which greatly reduces the computational cost.

3. Ignition in a quiescent mixture (1D, spherical symmetry)

We first consider the ignition and subsequent flame propagation induced by a hot particle in a quiescent stoichiometric DME/air mixture at $P = 1$ atm and $T_u = 480$ K. According to [3], for a particle with radius of $R = 1$ mm and temperature in the range of $T_P = 1000\sim1500$ K, the temperature drop is within 2% during 100 ms. Therefore, it is reasonable to assume constant particle surface temperature.

Figure 2(a) shows the temporal evolution of total heat release rate for $T_P = 1200$ K. We observe a first-stage ignition due to LTC occurring around $r = 0.15$ cm, where the temperature is within the negative temperature coefficient (NTC) region and corresponds to the shortest first-stage ignition delay time. A premixed cool flame is first initiated and propagates outwards with a propagation speed of around 6 cm/s. The fuel passing through the cool flame is only partially oxidized by reactions involved in LTC. Around the particle surface with the highest temperature autoignition due to HTC occurs at around $t = 118$ ms resulting in an outwardly propagating premixed hot flame. During a short period, the hot flame propagates behind the leading cool flame establishing a double-flame structure with coexisting premixed cool and hot flames (also see Fig. S4 in the Supplementary Document). Since
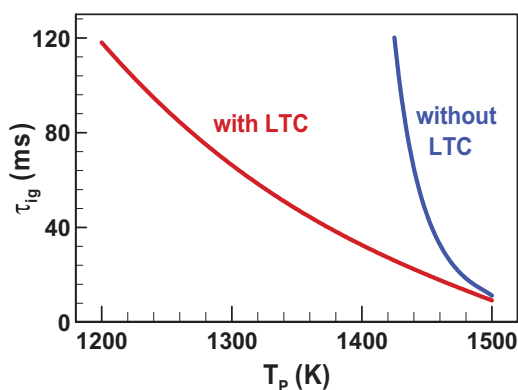
Fig. 3. Change of ignition time with particle surface temperature.

the hot flame is much stronger than the cool flame, the hot flame catches up and merges with the leading cool flame. Similar observation was reported by Zhang et al. [33]. Finally, only the hot flame exists and it propagates with a propagation speed of around 540 cm/s. Unlike previous studies on hot-particle induced ignition, the premixed cool flame and the double-flame structure are observed in the present simulations.

To demonstrate the effects of LTC, we conduct the simulations using the same kinetic model excluding the LTC listed in Table S1 of the Supplementary Document. For $T_P = 1200$ K without considering LTC, the hot flame cannot be ignited within 1000 ms. So Fig. 2(b) shows the results for a higher particle temperature of $T_P = 1425$ K. As expected, only the hot flame is initiated. The hot flame starts to propagate outwards at around $t = 120$ ms, which is slightly longer than $t = 118$ ms for a much lower particle temperature of $T_P = 1200$ K but with LTC. Nevertheless, the hot flame propagation speed remains at around 540 m/s. Therefore, LTC can greatly accelerate the hot-particle induced ignition but it does not affect the hot flame propagation speed.

To further demonstrate the effects of LTC on ignition by hot particles, Fig. 3 compares the ignition delay time, τ_{ig}, obtained from the kinetic model with and without LTC. Here τ_{ig} is defined as the instant when the maximum temperature is 100 K higher than the particle temperature (i.e., $T_{max} = T_P + 100$ K). Since $T_P > 1200$ K, τ_{ig} corresponds to the ignition delay time for the hot flame rather than the cool flame. Note that the 0D homogeneous ignition delay time is about two orders of magnitude shorter than τ_{ig} shown in Fig. 3 for hot-particle induced ignition. Fig. 3 shows that τ_{ig} increases rapidly as the particle temperature T_P decreases. For $T_P < 1425$ K, successful ignition cannot be achieved within 150 ms when the LTC is not

included. At $T_P = 1425$ K, the ignition time from the kinetic model with LTC is $\tau_{ig} = 25.9$ ms, which is about one-fifth of $\tau_{ig} = 120.1$ ms for the case without LTC. However, at $T_P = 1500$ K, the LTC has only little influence on τ_{ig}. Therefore, Fig. 3 further shows that the LTC can greatly accelerate ignition by hot particles in certain particle temperature ranges. For a smaller particle, a higher particle temperature is required to ensure successful ignition and thereby the LTC effect becomes weaker according to Fig. 3.

To explain the effects of LTC on hot particle induced ignition, the temperature and OH mole fraction profiles are plotted in Fig. 4. Two particle temperatures of $T_P = 1300$ K and 1500 K are considered, for which the LTC has great and little effect, respectively. For $T_P = 1300$ K with LTC, at $t = 5$ ms, a local peak of OH radicals appears around $r = 0.18$ cm where the local temperature is within the NTC region. To identify the main reaction pathways for OH radical, we plot the net production rate of OH (ω_{OH}) and the contributions from different reactions for $T_P = 1300$ K with LTC at $t = 10$ ms in Fig. 5. The OH radical is shown to be produced mainly through LTC reactions $O_2CH_2OCH_2O_2H = HO_2CH_2OCHO + OH$ (R1), $HO_2CH_2OCHO = OCH_2OCHO + OH$ (R2) and $CH_2OCH_2O_2H = OH + CH_2O + CH_2O$ (R3). The contributions of intermediate-temperature reaction $H_2O_2(+M) = OH + OH(+M)$ (R4) and high-temperature reaction $H + O_2 = O + OH$ (R5) are negligible. Therefore, the local OH peak is due to LTC. Around the particle surface, the temperature is close to $T_P = 1300$ K and OH is produced by HTC. The local maximum OH concentration at $r = 0.18$ cm is about one-order lower than that around the particle surface. Nevertheless, it reduces the diffusive flux of OH radicals from the HTC reaction zone to the surrounding mixture. Fig. 4(a) shows that at $t = 10$ and 15 ms, the OH mole fraction near the particle is higher when the LTC is included, indicating that the LTC results in an OH radical pool barrier surrounding the particle surface where HTC autoignition occurs. This barrier reduces the diffusive loss of radicals like OH from the HTC reaction zone. Consequently, the HTC autoignition becomes much shorter when the LTC is included.

For a higher particle temperature of $T_P = 1500$ K, Fig. 4(b) shows that the mole fraction of OH produced by HTC around the particle surface is about two-order higher than the local OH peak due to LTC at $t = 1$ ms. Moreover, the HTC autoignition time becomes much shorter and so does the diffusion time. Consequently, the barrier due to LTC has little influence on the HTC autoignition around the particle surface, and the profiles of T and X_{OH} near the particle surface are almost the same for cases with and without LTC. This explains why the LTC can greatly accelerate
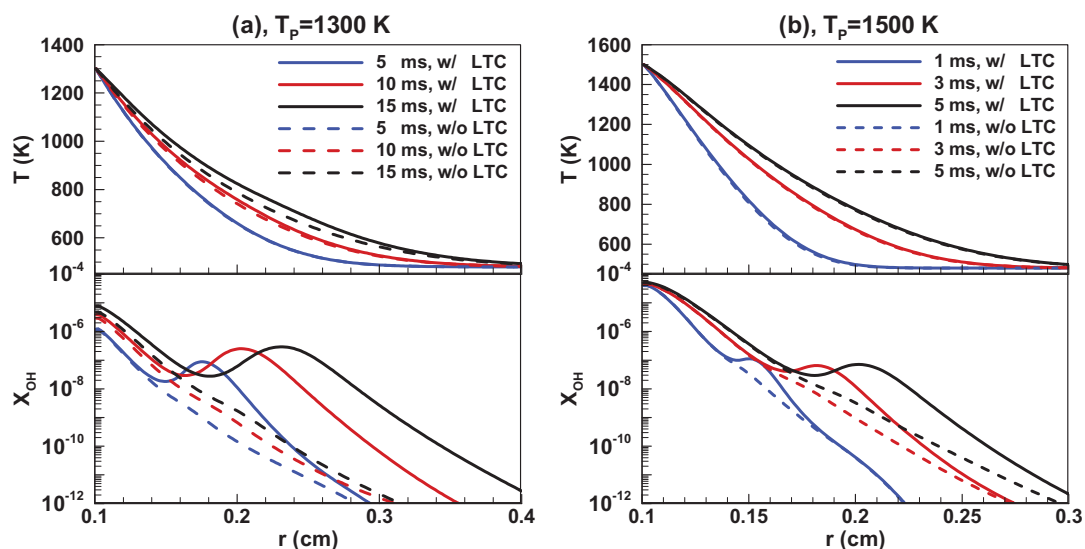
Fig. 4. Temperature and mole fraction of OH profiles for (a) $T_P = 1300\,K$ and (b) $T_P = 1500\,K$. Solid and dashed lines correspond to cases with and without LTC, respectively.
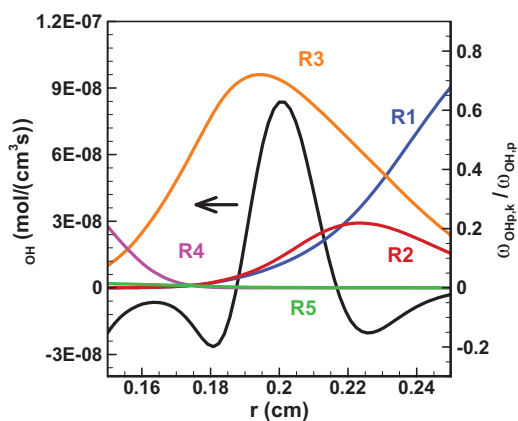

Fig. 5. The distributions of the net OH production rate and the contribution from reactions R1-R5 for $T_P = 1300\,K$ with LTC at $t = 10\,ms$.

particle ignition for $T_P = 1300\,K$ while it has little effect for $T_P = 1500\,K$ as shown in Fig. 3.

4. Ignition in a flowing mixture (2D, axial symmetry)

In quiescent mixtures the ignition is not affected by convective heat and mass transfer. In this section, we consider the relative velocity between the hot particle and flammable mixture.

Figure 6 shows the results for a typical case with uniform inlet flow speed of $u_{in} = 0.15\,m/s$.

The particle temperature is $T_P = 1400\,K$ and the LTC is included in the simulations. As a main product from LTC, CH_2O is chosen here to depict the premixed cool flame. At $t = 17\,ms$, a cool flame, represented by curve ABC on the Y_{CH2O} contour, is initiated and it propagates outwards. Due to the inflow, the cool flame has the lowest and highest absolute speed at upstream (point C) and downstream (point A), respectively. Since the LTC heat release is low, the temperature of the cool flame combustion products is only about 600 K and the thermal expansion ratio is about 1.25. Consequently, the cool flame has relatively minor influence on the flow and the streamlines are only slightly deflected by the weak gas expansion.

Figure 6(b) shows thermal runaway occurring at $t = 27.2\,ms$ due to HTC autoignition around the rear stagnation point, D. This is evidenced by the nearly complete consumption of CH_2O around point D. In previous studies [17,34], it was also observed that the ignition kernel first forms around the rear stagnation point with the thickest thermal boundary layer and the smallest heat and radical transport from the particle surface to the surroundings. At $t = 27.6\,ms$, a hot flame is fully formed which is represented by curve DEF in Fig. 6(c). Within the hot flame CH_2O is completely consumed. The hot flame starts to propagate after the leading cool flame and thereby the double-flame structure is observed. Since the hot flame is much stronger and faster than the cool flame, the hot flame at point F catches up and merges with the cool flame at C around $t = 28\,ms$, as shown in Fig. 6(d). Finally, the hot flame at D merges with the cool flame at A, and the cool
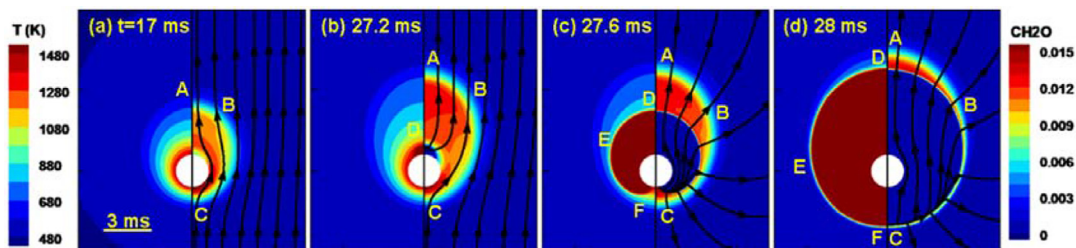
Fig. 6. Evolution of the temperature (left) and CH_2O mass fraction (right) contours for $T_P = 1400$ K and $u_{in} = 0.15$ m/s. The filled white circle represents the hot particle with radius of 1 mm. The streamlines are imposed on contours of CH_2O mass fraction. Curves ABC and DEF represents the cool and hot flames, respectively.
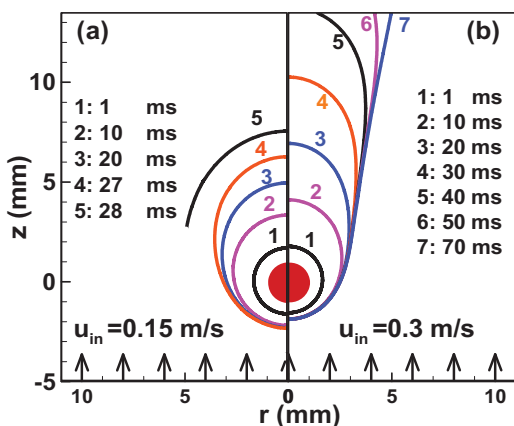

Fig. 7. Evolution of the cool flame front (iso-surface of $T = 600$ K) for (a) $u_{in} = 0.15$ m/s and (b) $u_{in} = 0.3$ m/s with $T_P = 1400$ K. The filled red circle represents the hot particle with radius of 1 mm.

flame completely disappears and only the hot flame survives. Fig. 7(a) shows the evolution of the cool flame front. At $t = 28$ ms (line #5 in Fig. 7(a)), part of the cool flame disappears after it is merged with the hot flame. The streamlines in Figs. 6(c) and 6(d) indicate that the flow is greatly affected by the thermal expansion due to the hot flame.

Figures 7(b) and 8 show the results for a higher inlet velocity of $u_{in} = 0.3$ m/s but the same particle temperature of $T_P = 1400$ K. It is observed that only the cool flame is initiated by the hot particle. The hot flame cannot be initiated due to the shorter residence time and larger convective loss of heat and radicals. An inverted flame cone eventually is stabilized between the hot particle and inlet fresh mixture. The results indicate that an isolated single cool flame can be stabilized by a hot particle under certain inlet flow velocities without O_3 addition. This kind of cool flame was not reported before and it merits further experimental studies.

Figure 9 shows the effect of the inlet flow velocity on ignition delay time τ_{ig} for $T_P = 1400$ K.

Again, τ_{ig} corresponds to the time for the initiation of the hot flame rather than the cool flame. It is interesting to observe that τ_{ig} first decreases and then increases abruptly with u_{in}. The hot flame cannot be initiated when u_{in} is above a critical value. A similar trend was also reported by Kobayashi et al. [35] studying the flow effects on the minimum ignition energy for laser-induced spark ignition in DME/air mixtures. This non-monotonic change indicates that the inlet flow has both positive and negative effects on the hot-particle ignition process. The negative effect comes from blowing the cool flame away from the rear stagnation point and destroying the radical pool built-up there for HTC autoignition. The positive effect comes from thickening the thermal boundary layer around the rear stagnation point and transporting radicals from upstream, which promote HTC autoignition near the rear stagnation point. The competition between the negative and positive effects of the inlet flow results in the non-monotonic change between τ_{ig} and u_{in}.

In order to test this hypothesis, we assess the effect of inlet flow velocity on the thermal boundary layer thickness behind the rear stagnation point. First, the simulation for $T_P = 1400$ K and $u_{in} = 0$ m/s is conducted to get the distributions for temperature and mass fraction of all species at $t = 1$ ms. These distributions are used as the initial conditions for different inlet velocities of $u_{in} = 0$, 0.1, 0.2, and 0.3 m/s. Additionally, simulations for a frozen flow without chemical reactions are conducted to assess the flow effect. Since the ignition kernel is formed first near the rear stagnation point, in Fig. 10 we plot the distributions of temperature and OH mass fraction along the vertical direction starting from the rear stagnation point. It is observed that the higher the inlet velocity, the larger the temperature and OH mass fraction within the thermal boundary layer. This confirms the hypothesis that higher inlet flow velocity contributes to a thicker thermal boundary layer behind the downstream particle surface.

Figure 9 also shows the results for $T_P = 1460$ K with and without LTC. The comparison indicates
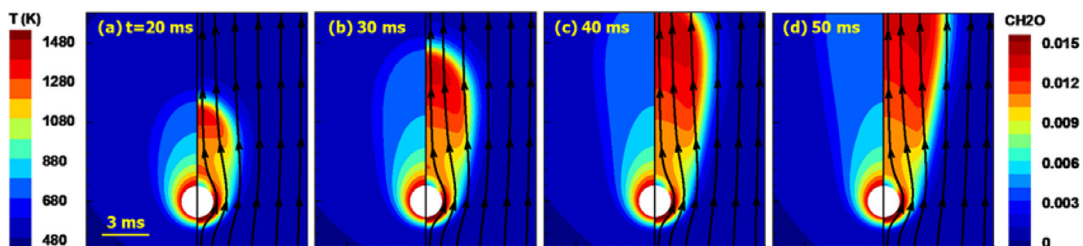
Fig. 8. Evolution of the temperature (left) and CH_2O mass fraction (right) contours for $T_P = 1400$ K and $u_{in} = 0.3$ m/s. The streamlines are imposed on contours of CH_2O mass fraction.
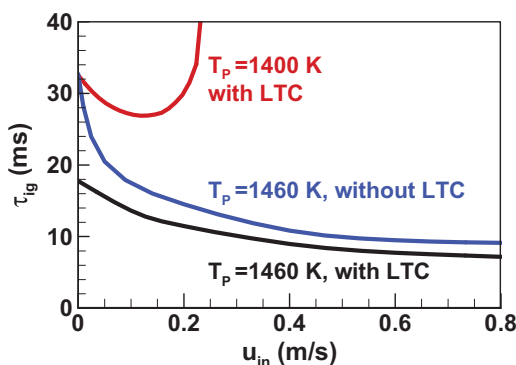

Fig. 9. Change of ignition time with inlet velocity for $T_P = 1400$ K and $T_P = 1460$ K.
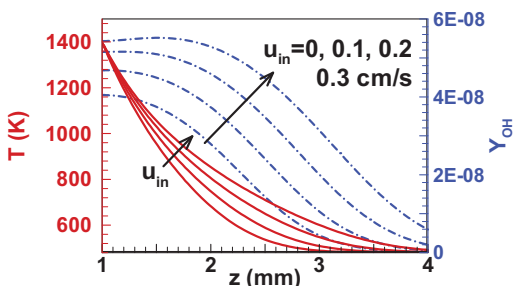

Fig. 10. Temperature (red solid lines) and OH mass fraction (blue dash-dotted lines) profiles along the vertical direction starting from the rear stagnation point for $u_{in} = 0$ m/s, 0.1 m/s, 0.2 m/s and 0.3 m/s at $t = 4$ ms. $T_P = 1400$ K.

that LTC can also accelerate the hot particle induced ignition in a flowing flammable mixture. However, with the increase of flow velocity, the ignition promotion due to LTC becomes weaker. This is because the radical barrier due to LTC (see Fig. 4(a) and related discussion) is pushed away from the rear stagnation point, where HTC autoignition first occurs, by the inlet flow. For $T_P = 1460$ K, Fig. 9 shows that the ignition time monotonically decreases with the increase of inlet

flow velocity for $u_{in} \leq 1$ m/s. It is expected that τ_{ig} increases with u_{in} for large value of u_{in}. However, as mentioned before, here we only consider $u_{in} \leq 1$ m/s so that there is not flow separation at the rear of the particle [17] and thus the problem remains 2D axissymmetrical. A Damköhler number with extended definition such as the inclusion of LTC-induced autoignition [36] might be helpful to interpret the phenomena observed in the 2D simulation.

All the above results are for DME/air at $T_u = 480$ K. Similar results are also obtained for other temperatures, e.g., $T_u = 600$ K as shown in Section S3 of the Supplementary Document. It is noted that the elevated temperature of $T_u = 480$ K is needed to get long-duration premixed cool flames. At room temperature, the time window for premixed cool flame is too short to be clearly analyzed [33] and the corresponding 2D computational cost is very large.

5. Conclusions

Hot particle ignition in quiescent and flowing stoichiometric DME/air mixtures are investigated through 1D and 2D numerical simulations, respectively. A detailed kinetic model including both LTC and HTC is used in the simulations. For the quiescent mixture, a premixed spherical cool flame is shown to be first initiated by the hot particle. During the slow propagation of the cool flame, HTC autoignition occurs near the particle surface, which triggers a hot flame propagating behind the cool flame. The double-flame structure for the coexistence of premixed cool and hot flames is observed. The hot flame catches up and merges with the leading cool flame. The LTC produces a radical barrier surrounding the particle surface which greatly reduces the diffusive loss of radicals like OH from the HTC reaction zone. Therefore, the LTC accelerates the HTC ignition of the stoichiometric DME/air mixture in certain particle temperature ranges.

For the flowing mixture, the premixed cool flame and the double-flame structure are also observed at certain inlet flow velocity ranges. At velocity of $u_{in} = 0.3$ m/s, only the cool flame is initiated by the hot particle while the hot flame cannot be ini-

tiated due to the shorter residence time and larger convective loss. This indicates that an isolated single cool flame might be stabilized by a hot particle under certain inlet flow velocity. The ignition time is shown to first decease and then increase rapidly with the inlet velocity. This non-monotonic change can be explained by the negative and positive effects of the inlet flow on ignition.

The present results demonstrate that the LTC plays an important role in hot particle ignition of DME/air mixtures. Future work will extent the inlet velocity to higher values so that the interaction between the local radical pool and flow recirculation zone can be studied. Besides, the coupling between buoyancy and LTC effects for low inlet flow velocity merits further study. Note that the present study is only computational and it needs to be explored experimentally in future studies.

Declaration of Competing Interest

None.

Acknowledgments

Supplementary materials

Supplementary material associated with this article can be found, in the online version, at doi: 10.1016/j.proci.2020.06.254.

References

[1] V. Babrauskas, *Ignition Handbook,,* Fire Science Publishers, Issaquah WA, 2003.

[2] B. Stack, A. Sepeda, M. Moosemiller, *Process Saf. Prog.* 33 (2014) 19–25.

[3] S.A. Coronel, *Thermal Ignition Using Moving Hot Particles*, Ph.D. thesis, California Institute of Technology, Pasadena, California, 2016.

[4] R.S. Silver, *Phil. Mag.* 23 (1937) 633–657.

[5] S. Paterson, *Phil. Mag.* 28 (1939) 1–23.

[6] S. Paterson, *Mag* 28 (1939) 1–23 na, Calif.

[7] J.W. Mullen II, J.B. Fenn, M.R. Irby, *Proc. Combust. Inst.* 3 (1948) 317–329.

[8] H.S. Homan, W.A. Sirignano, *Proc. Combust. Inst.* 18 (1981) 1709–1717.

[9] T.H. Dubaniewicz Jr, *J. Laser Appl* 18 (2006) 312–319.

[10] M. Beyer, D. Markus, *Sci. Technol. Energ. Mater.* 73 (2012) 1–7.

[11] F. Beyrau, M. Hadjipanayis, R. Lindstedt, *Proc. Combust. Inst.* 34 (2013) 2065–2072.

[12] D. Roth, P. Sharma, T. Haeber, R. Schiessl, H. Bockhorn, U. Maas, *Combust. Sci. Technol.* 186 (2014) 1606–1617.

[13] T. Häber, T. Zirwes, D. Roth, F. Zhang, H. Bockhorn, U. Maas, *Z. Phys. Chem.* 231 (2017) 1625–1654.

[14] S.A. Coronel, J. Melguizo-Gavilanes, S. Jones, J.E. Shepherd, *Exp. Therm. Fluid Sci.* 90 (2018) 76–83.

[15] S.A. Coronel, J. Melguizo-Gavilanes, R. Mével, J.E. Shepherd, *Combust. Flame* 192 (2018) 495–506.

[16] J. Melguizo-Gavilanes, S. Coronel, R. Mével, J. Shepherd, *Int. J. Hydrog. Energy* 42 (2017) 7380–7392.

[17] T. Zirwes, F. Zhang, T. Häber, H. Bockhorn, *Combust. Sci. Technol.* 191 (2019) 178–195.

[18] Y. Ju, C.B. Reuter, O.R. Yehia, T.I. Farouk, S.H. Won, *Prog. Energy Combust. Sci.* 75 (2019) 100787.

[19] T.I. Farouk, F.L. Dryer, *Combust. Flame* 161 (2014) 565–581.

[20] C.B. Reuter, V.R. Katta, O.R. Yehia, Y. Ju, *Proc. Combust. Inst.* 37 (2019) 1851–1859.

[21] C.B. Reuter, S.H. Won, Y. Ju, *Combust. Flame* 166 (2016) 125–132.

[22] S.K. Menon, P.A. Boettcher, B. Ventura, G. Blanquart, *Combust. Flame* 163 (2016) 42–53.

[23] R. Mével, K. Chatelain, P. Boettcher, G. Dayma, J. Shepherd, *Fuel* 126 (2014) 282–293.

[24] W. Hensel, K.L. Cashdollar, *Handbook of Explosion Prevention and Protection*, John Wiley & Sons, 2008.

[25] Z. Zhao, M. Chaos, A. Kazakov, F.L. Dryer, *Int. J. Chem. Kinet.* 40 (2008) 1–18.

[26] Z. Chen, M.P. Burke, Y. Ju, *Proc. Combust. Inst.* 32 (2009) 1253–1260.

[27] Z. Chen, *Combust. Flame* 157 (2010) 2267–2276.

[28] P. Dai, Z. Chen, *Combust. Flame* 162 (2015) 4183–4193.

[29] H.G. Weller, G. Tabor, H. Jasak, C. Fureby, *Comput. Phys.* 12 (1998) 620–631.

[30] T. Zirwes, F. Zhang, P. Habisreuther, M. Hansinger, H. Bockhorn, M. Pfitzner, D. Trimis, *Flow Turbul. Combust.* 104 (2020) 997–1027.

[31] D.G. Goodwin, H.K. Moffat, R.L. Speth, *Cantera: an Object-Oriented Software Toolkit For Chemical Kinetics, Thermodynamics, and Transport Processes*, Cantera Developers, Warrenville, IL, 2017 Version 2.3.0.

[32] T.J. Poinsot, S. Lelef, *J. Comput. Phys.* 101 (1992) 104–129.

[33] W. Zhang, M. Faqih, X. Gou, Z. Chen, *Combust. Flame* 187 (2018) 129–136.

[34] L.R. Boeck, M. Meijers, A. Kink, R. Mével, J.E. Shepherd, *Combust. Flame* 185 (2017) 265–277.

[35] Y. Kobayashi, S. Nakaya, M. Tsue, *Proc. Combust. Inst.* 37 (2019) 4127–4135.

[36] F. Hampp, R.P. Lindstedt, *Combust. Flame* 182 (2017) 248–268.

[37] Y. Wang, Z. Chen, *Combust. Sci. Technol.* (2020), doi:10.1080/00102202.2020.1788006.